



This is a repository copy of *In vitro low-fluence photodynamic therapy parameter screening using 3D tumor spheroids shows that fractionated light treatments enhance phototoxicity.*

White Rose Research Online URL for this paper:
<https://eprints.whiterose.ac.uk/179807/>

Version: Published Version

Article:

Aguilar Cosme, J.R., Gagui, D.C., Green, N.H. orcid.org/0000-0001-5413-0642 et al. (2 more authors) (2021) In vitro low-fluence photodynamic therapy parameter screening using 3D tumor spheroids shows that fractionated light treatments enhance phototoxicity. *ACS Biomaterials Science & Engineering*, 7 (11). pp. 5078-5089. ISSN 2373-9878

<https://doi.org/10.1021/acsbmaterials.1c00690>

Reuse

This article is distributed under the terms of the Creative Commons Attribution (CC BY) licence. This licence allows you to distribute, remix, tweak, and build upon the work, even commercially, as long as you credit the authors for the original work. More information and the full terms of the licence here:
<https://creativecommons.org/licenses/>

Takedown

If you consider content in White Rose Research Online to be in breach of UK law, please notify us by emailing eprints@whiterose.ac.uk including the URL of the record and the reason for the withdrawal request.



eprints@whiterose.ac.uk
<https://eprints.whiterose.ac.uk/>

In Vitro Low-Fluence Photodynamic Therapy Parameter Screening Using 3D Tumor Spheroids Shows that Fractionated Light Treatments Enhance Phototoxicity

Jose R. Aguilar Cosme, Dan C. Gagui, Nicola H. Green, Helen E. Bryant, and Frederik Claeysens*

Cite This: <https://doi.org/10.1021/acsbiomaterials.1c00690>

Read Online

ACCESS |



Metrics & More



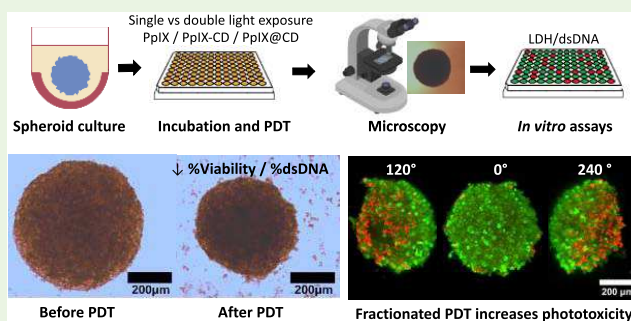
Article Recommendations



Supporting Information

ABSTRACT: The evaluation of novel photosensitizers (PSs) for photodynamic therapy (PDT) is difficult due to the limitations of two-dimensional cell culture and multiple parameters (dose, light intensity, uptake time), which complicate progression to *in vivo* experiments and clinical translation. Three-dimensional (3D) cell culture models like multicellular cancer tumor spheroids (MCTS) show great similarities to *in vivo* avascular tumor conditions, improving the speed and accuracy of screening novel compounds with various treatment combinations. In this study, we utilize C8161 human melanoma spheroids to screen PDT treatment combinations using protoporphyrin IX (PpIX) and drug-loaded carbon dot (CD) conjugates PpIX-CD and PpIX@CD at ultralow fluence values ($<10 \text{ J/cm}^2$). Conjugates show equivalent light-induced damage to PpIX from $1 \mu\text{g/mL}$ with significantly less dark cytotoxicity up to 72 h after exposure, shown by LDH release and dsDNA content. Fractionated treatments, carried out by dividing light exposure with 24 h intervals, demonstrate an enhanced PDT effect compared to single exposure at equal concentrations. Light sheet fluorescence microscopy combined with live/dead staining demonstrates that spheroids sustain extensive damage after PDT, with PpIX and PpIX-CD showing improved uptake compared to PpIX@CD. We show that PDT parameter screening can be carried out using a low-cost and convenient combination of assays to improve the efficiency of evaluating novel compounds.

KEYWORDS: photodynamic therapy, light fractionation, cancer spheroids, 3D cell culture, protoporphyrin IX, nanoparticles, carbon dots, light sheet fluorescence microscopy



INTRODUCTION

Photodynamic therapy (PDT) is an FDA-approved non-invasive cancer treatment that benefits from high site specificity, low cost, adaptability, and controlled dosimetry.¹ Photosensitizers (PSs) are compounds, which are capable of producing reactive oxygen species, including singlet oxygen ($^1\text{O}_2$), when irradiated with a specific wavelength of light, leading to internal damage and ultimately cell death.² However, many PSs cause off-target toxicity, have low water solubility, and rapidly undergo photobleaching, limiting their efficiency *in vivo*.³ In the 1980s, first generation PSs composed of porphyrins such as hematoporphyrin and porfimer sodium showed initial success but limited clinical use due to their unsuitable activation wavelengths and prolonged sensitization.⁴ Second generation PSs improved their function through chemical modifications, typically by altering functional groups. Other molecules were also investigated, including metalloporphyrins, phthalocyanines, chlorins, and dipyromethenes.⁵

In recent years, PS development has expanded beyond modifications to the molecular structure and synthesis of new compounds. The use of carriers such as antibodies,⁶ small targeting molecules,⁷ metal-organic frameworks⁸ and nano-

particles,⁹ has seen increased research interest, though testing of these novel agents is a complex task as there are a multitude of parameters to evaluate, such as light sources, irradiance, drug concentration, uptake time, and partial oxygen pressure.^{10,11} Among these carriers are carbon dots (CDs), highly biocompatible nanoparticles with tunable photoluminescence and surface chemistry, which have been previously used for PDT.¹²

Currently, *in vivo* tumor xenograft mouse models are the gold standard for PDT evaluation, often used early in the translational process with PS administered through subcutaneous injection or topical application; human tumor xenografts have also been explored for PS evaluation but are susceptible to infections. Animal models have been widely successful and

Received: May 23, 2021

Accepted: September 26, 2021

provide valuable insight as in the preclinical evaluation of novel compounds.¹³ However, they are hindered by strict regulatory controls, and the evaluation of multiple PDT treatment combinations is increasingly more difficult as more parameters are introduced, further complicating treatment standardization. Additionally, various PDT strategies have shown conflicting results clinically with standard PSs, such as the use of low-fluence light sources and fractionation—a clinical practice—whereby the total light dose is divided into two or more exposures separated by a period in the dark.^{14–16}

Thus, there is an urgent need for better models of PDT for *in vitro* PS evaluation prior to *in vivo* testing in animal models. Cell monolayers have been shown to be inefficient for drug evaluation as conditions such as diffusion rates, protein expression, and cell–cell interactions vary compared to *in vivo* tissue.¹⁷ Three-dimensional (3D) cell culture models are key to understanding tumor biology and developing new strategies for drug delivery, which consider the tissue architecture and microenvironment. There are various established models used for drug screening, which include organotypic tissue cultures from patients,¹⁸ scaffolds for tissue engineering,¹⁹ organoids,²⁰ and spheroids.²¹

Multicellular tumor spheroids (MCTS) are well-established 3D cell models, which resemble tumors morphologically and biologically. Spheroids can be grown using a variety of immortalized cell lines or patient-derived tissue samples.²² Their growth can be stimulated by preventing cells from attaching to a suitable surface, which promotes the formation of cell–cell interactions, production of extracellular matrix, and compaction. In turn, this leads to the formation of biologically relevant cell layers: an outer layer with rapidly proliferating cells, an intermediate layer with cells in a state of quiescence, and an inner necrotic layer caused by hypoxia and nutrient deficiency.²³ Spheroids have demonstrated greater similarity to responses from *in vivo* tumors compared to cell monolayers, showing higher drug resistance, cell–cell interactions, and heterogeneous uptake, making them valuable tools for *in vitro* evaluation of novel compounds.²⁴

Although PDT is limited by hypoxic inner regions, which lead to inefficient diffusion and the development of necrotic cores, spheroids have seen increasingly more research interest for PDT evaluation.²⁵ In particular, their cost-effectiveness, adaptability, ease of production, and similarities to *in vivo* tumors make them ideal for PDT parameter screening in comparison to cell monolayers.²⁶ Spheroid size is directly linked to drug resistance, with larger (500 μm) spheroids showing up to a 22-fold increase in drug resistance compared to cell monolayers with PDT.²⁷ Therefore, identifying an appropriate phase of spheroid development is crucial for evaluating drug phototoxicity. The three-dimensional structure of spheroids has been shown to influence reagent diffusion and drug uptake depending on a multitude of factors such as spheroids' size, cell type, and phase of the cell cycle, leading to poor reproducibility.²⁸ This significantly affects drug and nanoparticle distribution, as they typically rely on concentration gradients.²⁹

In this study, we present an *in vitro* 3D cell culture cancer spheroid model for evaluating PDT parameters for novel compounds, which combines biological assays and morphological assessment through microscopy. Our primary aim was to demonstrate the effectiveness of parameter screening using the combination of biological assays and microscopy. We demonstrate key differences in spheroids at 24–72 h after PDT

treatment using previously characterized carbon dot (CD)-protoporphyrin IX conjugates PpIX-CD and PpIX@CD.¹⁰ Additionally, fractionated treatments showed improved PDT-induced damage compared to single light exposures. Light sheet fluorescence microscopy was used to observe the drug uptake and morphological changes associated with phototoxicity. In summary, the combination of biological assays and microscopy improved the accuracy of parameter prediction in multicellular cancer spheroids compared to monolayer cell culture models while maintaining low cost, biological relevance, and ease of use.

EXPERIMENTAL SECTION

Materials. All chemicals were acquired from Sigma-Aldrich (United Kingdom) and used as received unless otherwise stated. Dulbecco's modified Eagle's medium (DMEM, high glucose), Dulbecco's modified Eagle's medium (DMEM, high glucose, without phenol red), fetal bovine serum (FBS), Quant-iT PicoGreen dsDNA quantification kit, Pierce LDH cytotoxicity assay kit, LIVE/DEAD Viability/Cytotoxicity Kit for mammalian cells, and trypsin-EDTA were obtained from Thermo Fisher (United Kingdom). Syringe filters with a 0.2 μm pore size were acquired from Sarstedt (United Kingdom), and 1 kDa MWCO, 6.4 mL/cm dialysis tubing was acquired from Spectrum Labs. Septa steel ring caps and 35 mL glass reaction vessels were obtained from CEM Corporation (United Kingdom). Deionized water was used for all buffers and samples in the experiments.

Sample Preparation. Carbon dots (CDs) and CD-PS conjugates were prepared using a previously described protocol.⁵ Briefly, CDs were synthesized via the microwave pyrolysis of citric acid or sucrose, with ethylenediamine as a passivating agent. PpIX was added during the microwave synthesis to produce S-guest embedded conjugates (PpIX@CD). Amide cross-linking was used to bind CDs and PpIX, obtaining cross-linked PpIX-CD. Conjugates were further processed by centrifuging at 5000 rpm for 30 min and dialyzing the solution using a 1 kDa molecular weight cutoff (MWCO), 6.4 mL/cm dialysis tubing to remove excess reagents and waste products.

Multicellular Tumor Spheroid Culture. Human melanoma cells (C8161) were cultured in phenol red-free DMEM with 10% fetal calf serum, 1% penicillin and streptomycin, and 1% L-glutamine. C8161 cells were cultured in a T75 flask at 37 °C, 5% CO₂ until around 80% confluence. Multicellular tumor spheroids were produced utilizing agar coating to prevent cell adhesion. A 1.5% agarose solution was prepared with 2-hydroxyethylagarose and standard cell culture media (DMEM). This solution was sterilized by autoclave and stored at 4 °C.

Agar-coated 96-well plates were prepared by adding 100 μL of the agarose solution into each well and leaving it to set at room temperature for at least 1 h. Plates were seeded with 100 μL of phenol red-free media containing 6×10^3 cells per well and returned to the incubator until the spheroids reached approximately 500 μm in diameter. Growth media was changed every third day, adding 100 μL to each well and removing an equal volume.

Photoactivation of CD-PS Conjugates. Spheroids were subjected to single and double light exposure periods with a mounted light-emitting diode (LED). CD-PS conjugates were first subjected to ultrasonic processing with a Hielscher UP50H ultrasonic probe prior to the dilution to remove aggregates and dissolved in phenol red-free media at a concentration of 50 $\mu\text{g}/\text{mL}$, being kept refrigerated until used. Stock solutions were placed in an ultrasonic water bath for 15 min at 37 °C. Spheroids were treated using conjugate dilutions to achieve concentrations of 1, 5, and 10 $\mu\text{g}/\text{mL}$ in a 200 μL volume. The plates were then returned to the incubator for 2 h to allow uptake.

A M405L2 ThorLabs mounted LED with a collimator adapter ($\lambda_{\text{ex}} = 405 \text{ nm}$, 1500 mA output, 2.76 mW/cm^2) was used to induce light-activated toxicity. Single exposure (1LT) samples were placed under illumination for 15, 30, and 60 min, corresponding to 2.5, 5, and 10 J/

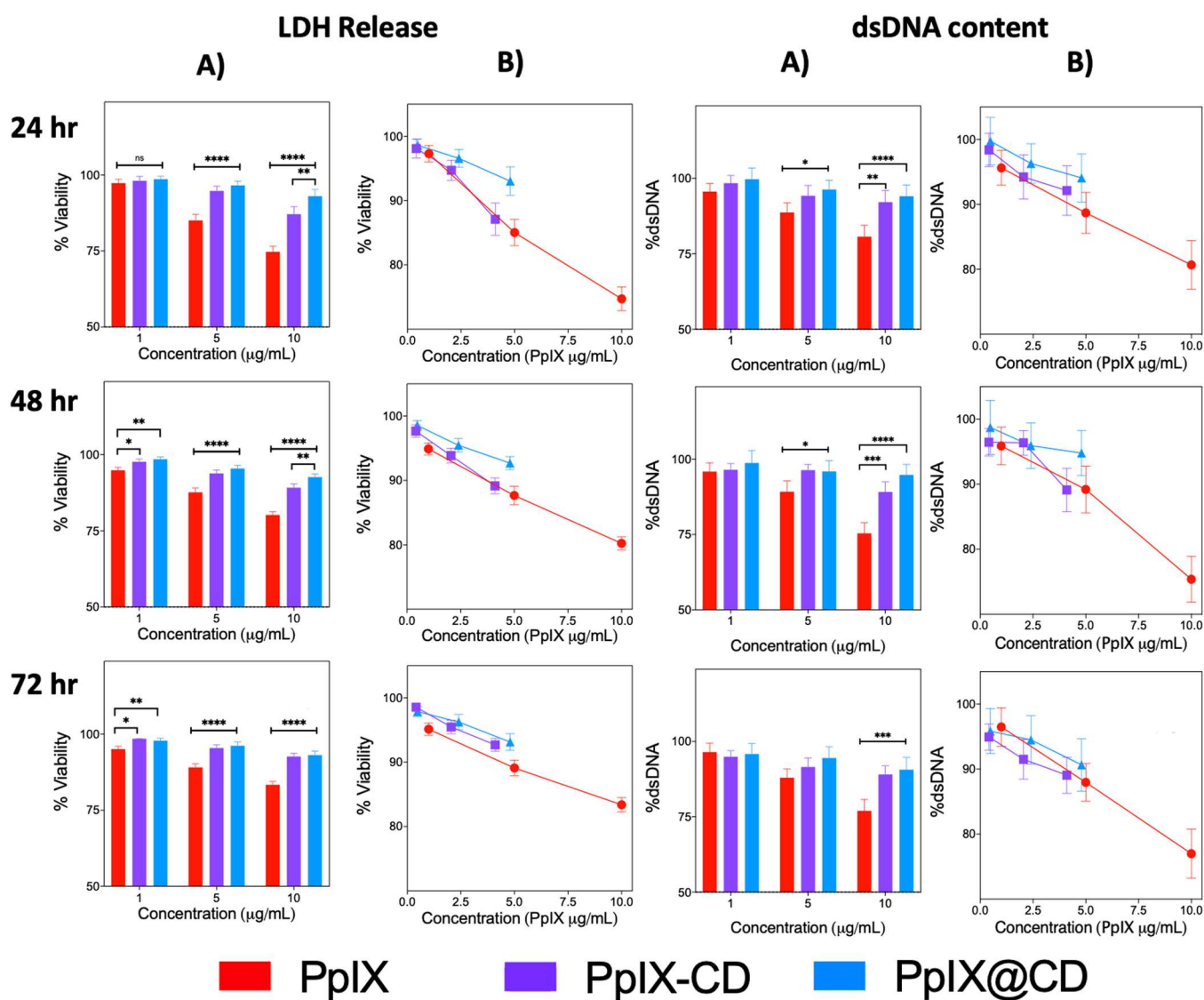


Figure 1. CD-PS dark toxicity in spheroids is similar, based on relative drug content. CD-PS samples decreased drug-induced cytotoxicity up to 72 h after incubation. LDH release showed CD conjugates caused less damage to the cell membrane compared to PpIX, with some variation in DNA content at concentrations of 1–10 $\mu\text{g/mL}$ (A). PpIX-adjusted values (PpIX $\mu\text{g/mL}$) based on the estimated drug content for each sample type demonstrate no variation regardless of concentration (B). Significance was calculated between CD-PS samples and PpIX in identical treatment conditions, where $*p < 0.05$. ($N = 3$, $n = 6$).

cm^2 , and subsequently returned to the incubator. Sequential light treatments (2LT) were carried out 24 h after the first light dose using the same methodology for 1LT. Media was removed and replaced immediately after each light exposure. LDH release and DNA quantification were measured at 24, 48, and 72 h time points (post final light activation). Control spheroids were also subjected to equal non-incubation conditions and light fluence rates as spheroids used in experimental groups.

LDH Release Assay. LDH release was measured in all samples by collecting 50 μL of media and transferring it to a 96-well plate. Spheroids which had not been treated with CD-PS conjugates but which were exposed to equal irradiation times were used as negative controls for spontaneous LDH release. The positive control was carried out by incubating spheroids with TE buffer (10 mM Tris-HCl, 1 mM EDTA, pH 7.5) for 45 min, followed by four freeze-thaw cycles (frozen 30 min at -80°C , thawed 10 min at room temperature) to ensure membrane disruption and indicate maximum LDH release.

Subsequently, 50 μL of LDH working solution was added to each well and covered to avoid exposure to light. Plates were incubated for 30 min, and 50 μL of LDH stop solution was added to finalize the

reaction. Briefly, 50 μL of liquid was taken from each well, and absorbance was read at 490 nm (LDH) and 680 nm (background) with a microplate reader (Bio Tek Instruments ELx800). Cytotoxicity was calculated with the following formula.

$$\% \text{ cytotoxicity} = \left(\frac{\text{sample LDH release} - \text{spontaneous LDH release}}{\text{maximum LDH release} - \text{spontaneous LDH release}} \right) \times 100$$

Viability was calculated using the following formula

$$\% \text{ viability} = \% \text{ cytotoxicity}_{\text{control}} - \% \text{ cytotoxicity}_{\text{sample}}$$

dsDNA Quantification Assay. PicoGreen working solution was prepared by dissolving the reagent in TE buffer (10 mM Tris-HCl, 1 mM EDTA, pH 7.5) according to the instructions from the manufacturer. Spheroids were removed from each well and placed in a 96-well plate and carefully washed three times with 50 μL of sterile phosphate-buffered saline (PBS) to remove cellular debris. Cell

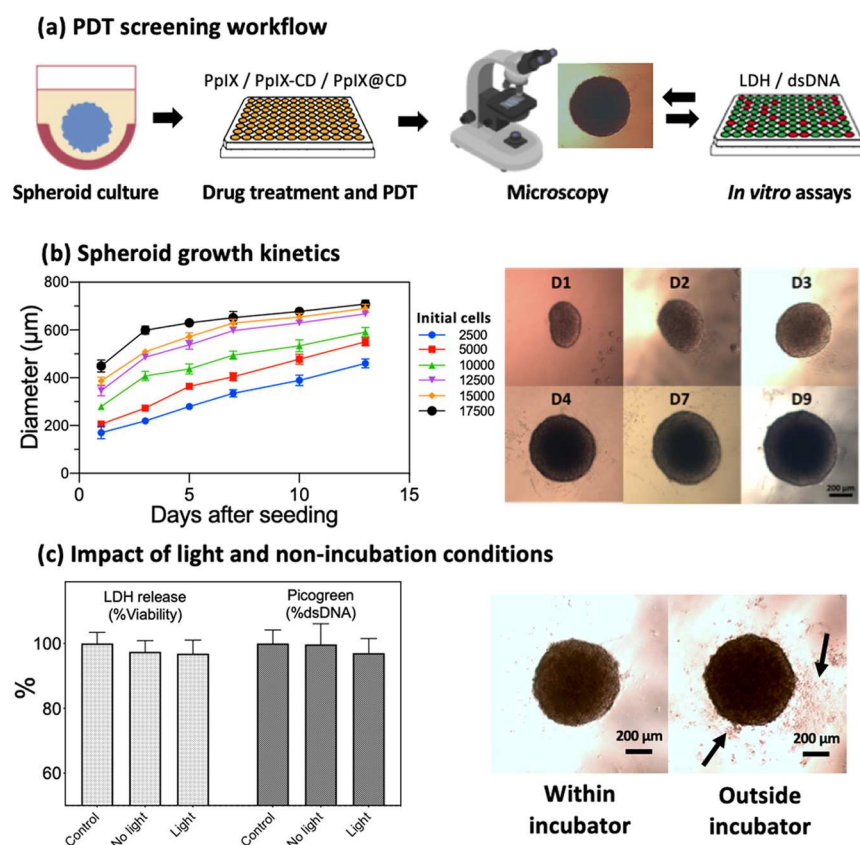


Figure 2. PDT screening was carried out after incubation with CD-PS conjugates. (a) Treatment efficiency was evaluated using a combination of microscopy and *in vitro* assays. (b) Spheroid growth varies according to initial seeding density and impacts PDT evaluation as spheroids progressively become rounder and larger after the initial 3-day growth period. Spheroids are not affected by 405 nm light and prolonged exposure outside incubation conditions. (c) PDT conditions for spheroids were tested by comparing control spheroids (no light, placed within normal incubation conditions) to samples placed outside the incubator (no light, 1 h) and samples exposed to a 405 nm LED light (2.76 mW/cm^2 , 10 J/cm^2). ($N = 3$, $n = 6$). The characteristic quasi-spherical morphology attained during spheroid growth was slightly affected by environmental stress, seen as debris surrounding the main aggregate indicated with arrows.

lysis was performed by adding $50 \mu\text{L}$ of TE buffer to each well and freeze-thawed four times, as detailed previously. An equivalent volume of $100 \mu\text{L}$ PicoGreen working solution was added. The plates were covered from light and incubated for 10 min at room temperature. Fluorescence was read at 485 nm excitation and 528 nm emission with a fluorescence plate reader (Bio Tek Instruments FLx800). A blank was prepared by adding deionized water and PicoGreen in equal volumes. % dsDNA was calculated with the following formula

$$\% \text{ dsDNA} = \left(\frac{\text{sample dsDNA} - \text{control dsDNA}}{\text{control dsDNA}} \right) \times 100$$

Light Microscopy (LM). Images were obtained using an AE2000 inverted light microscope (Motic) fitted with a Moticom 2.0 camera (2 MP) and a 4 \times objective. Images were obtained before and after clearing cellular debris from each well. White balance was optimized to increase spheroid contrast against the background.

Light Sheet Fluorescence Microscopy (LSFM). Prior to imaging, the spheroids were fixed with 3.7% paraformaldehyde and embedded in 1% 2-hydroxyethylagarose. LSFM was carried out with a ZEISS Lightsheet Z.1 microscope (ZEISS, United Kingdom) fitted with a W Plan-Apochromat 10 \times objective. Images were obtained as Z-stacks with a $1.8 \mu\text{m}$ slice interval and a stack size of $878.09 \mu\text{m} \times 878.09 \mu\text{m}$. Light sheet thickness was adjusted to $6.4 \mu\text{m}$, and the pixel size was $0.46 \mu\text{m}$.

Image processing was carried out using ZEISS ZEN 2014 SP1 software version 9.2.0.0 and ImageJ. The image acquisition settings (excitation/emission wavelengths and other adjustments) for live/

dead microscopy and drug uptake analysis are described in detail below.

Live/Dead Microscopy. Cells were stained with $2 \mu\text{M}$ calcein AM reagent and $4 \mu\text{M}$ ethidium homodimer-1 to differentiate live and dead cells. Staining solutions were prepared on the day of use to avoid the spontaneous hydrolysis of calcein AM due to moisture. Spheroids were moved to new wells and gently washed with PBS before adding $100 \mu\text{L}$ of staining solution. The plates were left at room temperature for 45 min before washing with PBS and storing at $4 \text{ }^\circ\text{C}$.

LSFM was carried out with the following: a 405/488/561/640 nm laser blocking filter, an SBS 560 nm long-pass filter. Images were captured simultaneously: Calcein AM (detected in the 505–545 nm range using a bandpass filter) and ethidium homodimer-1 (detected above 660 nm using a long-pass filter). A 448 nm laser was used at 0.6% power with 119.85 ms exposure time for both fluorophores. Each spheroid was imaged at 0, 120, and 240° with the same parameters.

Drug Uptake Analysis. After a 3 h uptake period, the spheroids were fixed with 3.7% paraformaldehyde and embedded within 1% 2-hydroxyethylagarose. LSFM was carried out with the following: a 405/488/561/640 nm laser blocking filter, an SBS 560 nm long-pass filter. A 405 nm laser (5% power and $199.7 \mu\text{s}$ exposure time) was used to acquire images. Fluorescence intensity was measured within the innermost section of the spheroid as determined by Z-stacks (2 μm interval).

Scanning Electron Microscopy (SEM). Spheroids fixed in 3.7% paraformaldehyde, as described above, were washed twice in PBS at intervals of 10 min. Afterward, they were fixed a second time in 1% aqueous osmium tetroxide for 1 h at room temperature before

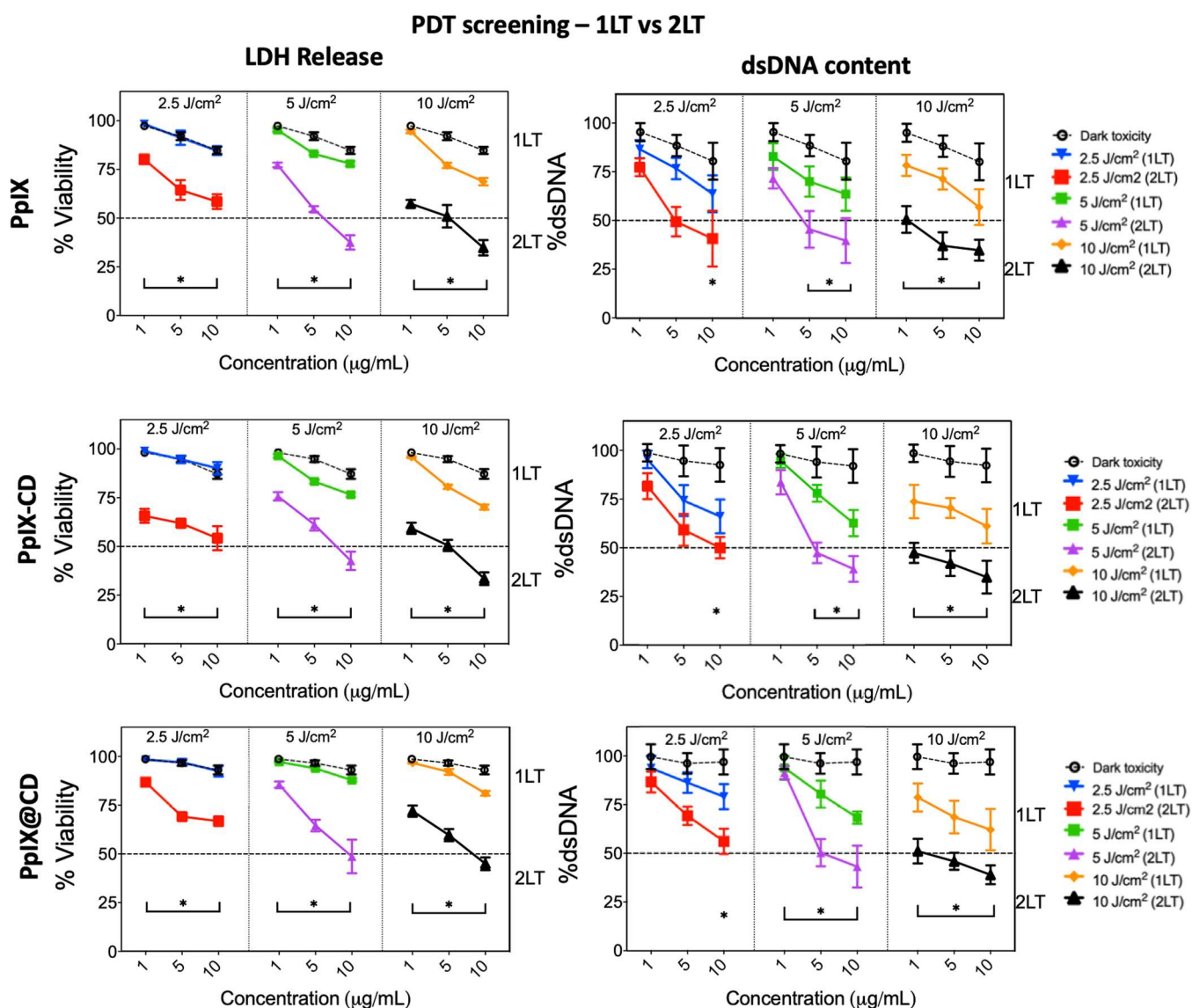


Figure 3. Fractionated PDT improves PDT effectiveness using lower fluence rates and concentrations. Phototoxicity was evaluated 24 h after exposure using LDH release and total dsDNA content. Light treatment combinations (1LT and 2LT) were compared based on total fluence (2.5–10 J/cm²) using equal PS concentrations (µg/mL). Control spheroids were subjected to the same conditions and used to indicate normal spheroid response. Data was normalized using the negative control (no light, no drug) as 100% and total spheroid disruption as 0%. Significance was calculated between 1LT and 2LT conditions at equal concentrations, where **p* < 0.05. (*N* = 3, *n* = 6).

undergoing two more PBS washes. Samples were exposed to an ethanol series at room temperature at 15 min intervals (75, 95, 100, 100% dried over anhydrous copper sulfate). Each sample was placed in a 50/50 mixture of 100% ethanol/100% hexamethyldisilazane for 30 min, followed by 30 min in 100% hexamethyldisilazane. Spheroids were air-dried overnight in a fume-hood and coated with gold in an Edwards S150B sputter coater. SEM micrographs were obtained using TESCAN Vega 3 LMU scanning electron microscope at an accelerating voltage of 20 kV.

Statistical Analysis. Experiments were carried out with three independent repeats in sextuplicate (*N* = 3, *n* = 6), and results were normalized against untreated control spheroids. Statistical analysis was done using GraphPad Prism version 8.3.0. Results obtained from biological assays (LDH and dsDNA quantification) from spheroids in identical conditions were evaluated by 2-way ANOVA analysis with Dunnett's test for multiple comparisons, with adjusted *p* values < 0.05 considered statistically significant. Data are presented as means ± standard deviation (SD).

RESULTS

In Vitro Evaluation of Dark Toxicity in Spheroids. Cell culture and scheduling of PDT treatment were optimized such that the spheroids were treated when they contained a proliferative rim and small necrotic core and were in the growth phase. We utilized previously reported PpIX-based nanoparticle conjugates to evaluate the PDT response in spheroids compared to cell monolayers, based on a pre-established concentration range of 1–10 µg/mL.⁵

As can be seen in Figure 1, conjugation slightly reduces dark toxicity (approx. 20%), as evidenced by LHD release and dsDNA content after adjusting for PpIX concentration. This was only observed at higher concentrations (>5 µg/mL), with the spheroids recovering after 48 h of incubation. Drug concentration was also adjusted based on relative drug content in each sample from the previous characterization and expressed as PpIX µg/mL (Supporting Table S1). Dark

toxicity showed similar drops in both assays as drug concentrations were increased, which were considered as PDT parameters were selected.

In Vitro Evaluation of Phototoxicity in Spheroids.

Phototoxicity in spheroids was evaluated with variations in fluence and drug doses. The maximum light dose was selected by examining LDH release, dsDNA content, and spheroid morphology, following both a single fraction (1LT) and double fraction (2LT) exposure with untreated spheroids (Figure 2). Spheroids did not show a significant difference after exposure to non-incubation conditions or light exposure for periods of up to 1 h. Spheroids were consequently incubated with PSs and exposed to increasing doses of light, up to 10 J/cm². Cell death can be observed as a halo of debris surrounding the spheroid, which changes in abundance depending on the degree of damage sustained after PDT (Supporting Figure S1). Growth media was replaced to slowly remove debris from each well, though this became more difficult with increasing damage, with some spheroids breaking upon rinsing. Low conjugate doses (1 μg/mL) combined with low fluence (2.5 J/cm²) showed a limited PDT effect.

The increase of both conjugate concentration and irradiance increased photoinduced damage, though there was increased resistance to compound toxicity as spheroids treated with 2.5 J/cm² (1LT) did not show a significant difference from nonirradiated spheroids. PpIX-CD consistently outperformed the other samples at most conditions, though this was only observed at 24 and 48 h post PDT. Spheroid damage could be observed up to 72 h after the last light treatment (Supporting Figures S2 and S3). PpIX@CD showed poor effectiveness at 1 μg/mL for LDH release but demonstrated an equal effect to both PpIX-CD and PpIX during DNA quantification. PpIX-loaded conjugates were able to provoke a similar degree of damage in spheroids compared to PpIX in both assays.

There was a significant difference in observed viability values derived by LDH release and DNA concentration at low light doses and drug concentrations (Figure 3). LDH values (% viability) were significantly different between 1LT and 2LT, regardless of the sample or treatment conditions. In contrast, the total dsDNA exhibits no significant change, particularly at 2.5 J/cm² and 1–5 μg/mL. 1LT was unable to consistently reduce spheroid viability and DNA content below the 50% threshold, though high drug/light combinations (1LT with >5 μg/mL and 5 J/cm²) were shown to be significantly more effective compared to low doses. Fractionated PDT showed a slight variation between light doses: while LDH release is significantly higher in fractionated treatments, this was not always observed with dsDNA quantification. Some variations can be seen at higher concentrations (>5 μg/mL) or light exposure (>5 J/cm²). Nonetheless, PpIX and conjugates do not show a significantly different PDT effect at equal concentrations and light doses (Supporting Figure S4).

Subsequently, we compared the total radiant exposure in equivalent treatments, e.g., a single 5 J/cm² exposure versus a double fractionated 2.5 J/cm² exposure (Figure 4). In total, 54 parameter combinations were evaluated using MCTS at three distinct time points, showing variations in spheroid viability according to treatments (Supporting Table S2). LDH release was significantly affected by sequential exposures, with all conditions showing improvement over single light treatments regardless of fluence, concentration, and sample type. In contrast, dsDNA quantification showed minimal differences between treatments. Single light treatments (1LT) proved to

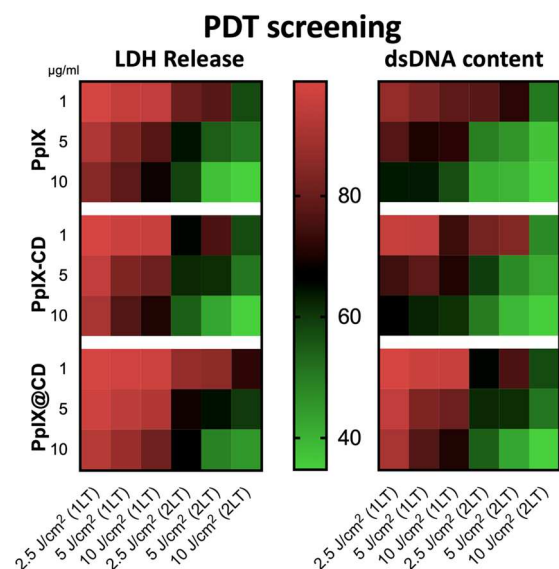


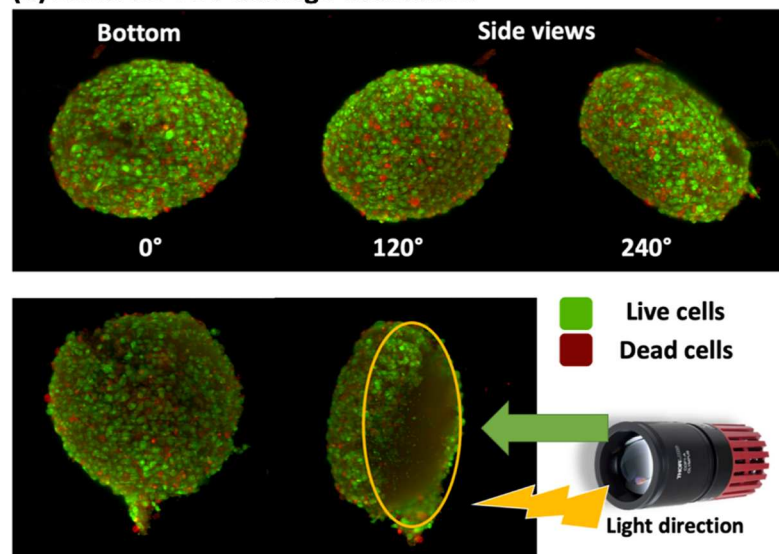
Figure 4. Summary of PDT parameter screening by treatment effectiveness. Lower values (green) indicate greater damage to spheroids after light exposure.

be unreliable unless higher drug concentrations were added, which increased sample variation due to dark toxicity from samples. Fractionated treatments (2LT) were shown to be slightly more effective at lower drug concentrations.

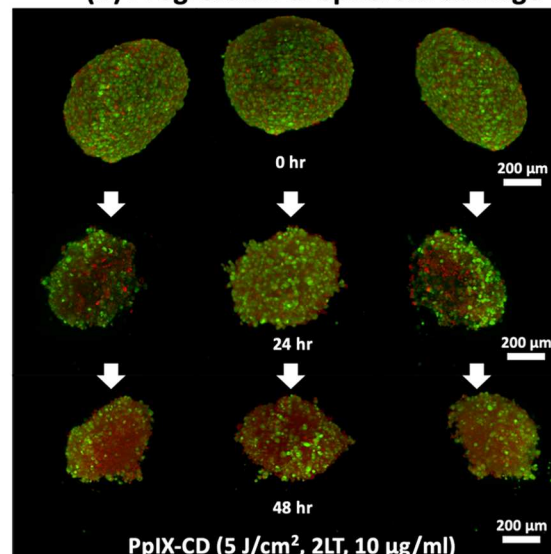
PpIX-adjusted values reveal similar results to those previously observed in cell monolayers. PS concentrations higher than 1 μg/mL produce greater spheroid damage in both 1LT and 2LT conditions using 41–48% PpIX. In combination with the previously shown dark toxicity data, these results can be used to rapidly contrast all treatment conditions to select suitable combinations for further evaluation. As can be seen in Figure 4, 1LT treatments showed poor PDT effectiveness regardless of fluence, concentration, and sample type. While higher-end single light exposure conditions (5–10 μg/mL, 10 J/cm²) can cross the 80% viability threshold, they are unsuitable as these PS concentrations already cause up to 25% drops in viability due to dark toxicity. In contrast, 2LT treatment combinations generally produced much greater damage across all parameters, with only 1 μg/mL conditions showing similar results to 1LT. Similarly, high PS concentrations were not found to be suitable due to dark toxicity, indicating a drug dose around 5 μg/mL combined with >2.5 J/cm² (2LT) is the most suitable treatment condition for producing a greater PDT effect while limiting the impact of PS toxicity.

Quantification of Conjugate Uptake. Light sheet fluorescence microscopy was used to estimate drug uptake in spheroids. Spheroids showed some autofluorescence at 405 nm excitation, though a 560 nm long-pass filter ensured that the control did not show any appreciable fluorescence emission after 600 nm. Conversely, spheroids incubated with all samples and doses (1–10 μg/mL) for 3 h showed clear emission peaks. Low sample concentrations (1 μg/mL) resulted in uptake within the spheroid periphery. In contrast, PpIX@CD showed aggregation within one side of the outermost layer of the spheroid and low emission in the other areas (Figure 5). The adjustment of concentration to 5 μg/mL corresponds to a considerable increase of fluorescence from all samples. PpIX-CD displayed markedly higher emissions in comparison to the

(a) LSFM for PDT damage evaluation



(b) Progression of spheroid damage



(c) Evaluation of drug uptake

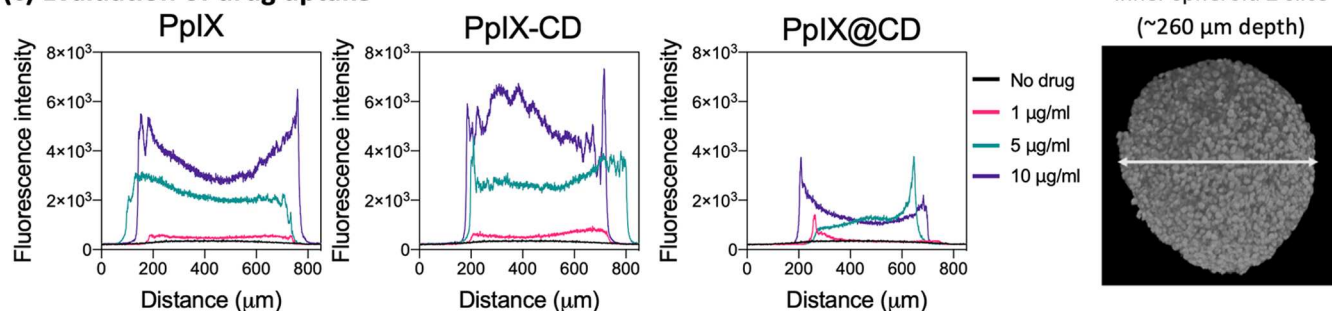


Figure 5. Spheroids show directional damage to their morphology after PDT. (a) Post-PDT morphology varies according to viewing angle, showing significant cell death throughout their structure after 24 h. (b) Increased drug doses destabilize spheroid morphology and cause ongoing cell death after 24 h of PDT (5 J/cm², 2LT, 10 μg/mL), with further cell death observed up to 48 h after the second light treatment. Initial damage was like that found in 1LT (middle) and continued to reduce spheroid size while increasing cell death (bottom). (c) Drug uptake in spheroids varies by sample type and concentration. CD-PS conjugate internalization within spheroids was observed using the middlemost Z-stack image obtained with light sheet fluorescence microscopy. Relative PpIX concentration is shown as fluorescence intensity across the innermost spheroid region (~260 μm depth). Spheroids were incubated with conjugates for 3 h and fixed prior to imaging.

control PpIX, with approximately 28% more uptake. PpIX-CD also showed similar values along the innermost part of the spheroid. In comparison, PpIX@CD continued to show much lower PpIX accumulation, with only 49–60% emission in comparison to PpIX and PpIX-CD, indicating possible self-quenching due to its cargo (Supporting Table S3). The embedded conjugate once again showed higher uptake in one side of the spheroid, with drastically reduced emissions on the opposite sides. This behavior continued as conjugate concentration increased to 10 μg/mL, though emissions were only increased 2-fold, compared to 10-fold between 1 and 5 μg/mL.

Observation of PDT-Induced Damage in Spheroids.

The distribution of live/dead cells within MCTS was observed using LSFM (Figure 5 and Supporting Figure S6). Spheroid morphology appeared to remain intact from initial viewing angles, though changes in viewing angles demonstrated the extent of PDT-induced damage. Imaging shows treated spheroids have reduced size and slightly irregular morphology but generally keep their roundness regardless of light treatment, as shown previously. Images were obtained from three separate angles to observe morphology after PDT with 5

J/cm², which was a light dose, which produced significant damage to the spheroids while reducing time spent outside the incubator. Drug doses (1–10 μg/mL) and fractionated light exposures (1LT and 2LT) were left unchanged from the previous methodology. Samples using 1 μg/mL did not show significant changes to roundness, with only small sections being affected, regardless of light dose. Nonetheless, sample rotation revealed changes in spheroid thickness, which was reduced from ~450 to ~400 μm because of PDT-induced cell death.

PDT with a concentration of 5 μg/mL significantly increased damage to the spheroids and caused disruption in their spherical shape. PpIX and PpIX-CD show damage throughout the spheroid surface, appearing as large grooves that run across its diameter and missing sections corresponding to the area which was in contact with light. The core area of all spheroids showed a high number of dead cells, which corresponds to the hypoxic region formed during initial growth and compaction. The spheroid shape was also influenced by sample manipulation during fixing and mounting, as samples frequently needed to be swapped as too much force caused the spheroids to begin falling apart. In

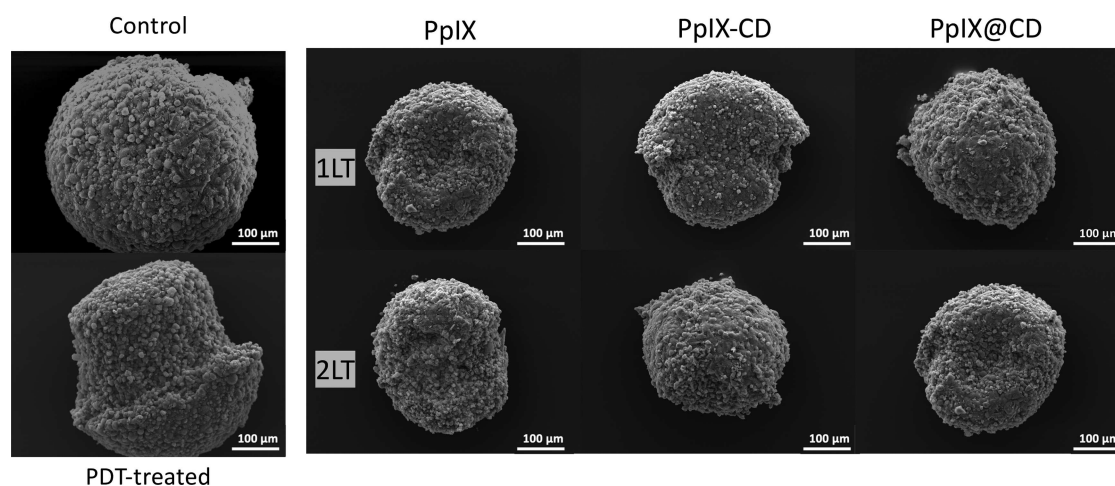


Figure 6. Standard C8161 melanoma spheroid imaged using SEM. SEM micrographs were taken at 500 \times magnification. Control spheroids show some slight damage (visible in the top right corner of the image) due to manipulation during fixation. PDT-treated spheroids underwent directed light-activated damage after exposure to light. Images correspond to spheroids treated with 5 $\mu\text{g}/\text{mL}$ conjugates, 1LT/2LT, 24 h after exposure. The effect of PDT can be seen as sloughing of outer cell layers increased due to increased damage from 1LT and 2LT PDT.

comparison, spheroids treated with 10 $\mu\text{g}/\text{mL}$ show more pronounced damage and a similar loss of shape and roundness. However, it should be noted that not all spheroids within the same conditions showed the same degree of damage.

SEM imaging has been used to observe fine details in spheroid morphology, revealing cell–cell interactions and growth progression with higher magnifications. We used surface morphology as an indicator of morphological changes not immediately apparent after observation with LM. Control spheroids show a clear round morphology reminiscent of images obtained with LM, with few defects on their surface. In contrast, PDT-treated spheroids show clear deformation after treatment as ROS production and subsequent cell death changes spheroid morphology. The previously described surface sloughing and deformation can be seen in the representative images shown in Figure 6.

DISCUSSION

The development of a spheroid-based model for PDT is difficult due to variability during the initial stages of growth and the wide variety of available assays for biological assessment, which hinder standardization. PDT is highly dependent on PS concentration, tissue penetration, and oxygen availability. The first step was to determine the ideal spheroid size to screen treatment conditions. Spheroids under 200 μm typically have proliferating and quiescent cells, while those around 300 μm begin to show signs of hypoxia in their centers. Furthermore, the diffusion limit of molecules such as oxygen is 150–200 μm , leading to the formation of a necrotic core within 4–10 days, depending on cell type and initial seeding density. Therefore, we made use of larger spheroids (>500 μm), which have a higher degree of similarity to murine xenografts in cell cycle and apoptosis (Supporting Figure S1).³⁰ Additionally, they have also shown increased drug resistance in comparison to smaller aggregates (<300 μm) through a combination of necrosis and hypoxia.³¹ Dark toxicity was not found to be substantially different in spheroids after adjusting concentrations based on relative drug content (Figure 1). Our results are similar to those reported by Pereira et al. (2017), who determined that tetraglycosylated

porphyrin PorGlu4 had no significant difference in monolayers versus spheroids up to 9 μM (5 $\mu\text{g}/\text{mL}$).²⁶

The evaluation of PDT parameters with spheroids required us to adjust previous fluence values from those used in monolayers. Previous experiments showed up to a 50% reduction in metabolic activity in C8161 monolayers treated with 1 $\mu\text{g}/\text{mL}$ PpIX at 0.83 J/cm^2 at 405 nm. Conjugates showed similar results with monolayers: PpIX-CD (LD50—1.9 $\mu\text{g}/\text{mL}$) and PpIX@CD (LD50—1.6 $\mu\text{g}/\text{mL}$).¹⁰ In contrast, spheroids did not respond to the previous experimental conditions until fluence was increased to 2.5 J/cm^2 . Thus, the fluence range was set to the range of 2.5–10 J/cm^2 . While 405 nm light is of limited utility in clinical applications due to poor tissue penetration, there are some benefits to its use for research on the choice of illumination parameters. Helander et al. (2014) demonstrated that using blue light (410 nm) to carry out PDT with hexyl 5-aminolevulinic acid was better than red light (624 nm) at producing cell death in various cancer cell lines, though red light induced more apoptosis, highlighting the importance of evaluating sublethal light doses in PDT.³²

Total light exposure remained within the ultralow fluence range previously utilized by Matthews et al. (2009) to deliver sublethal light doses to human glioma spheroids with ALA at 1.5–6 J/cm^2 .^{2,33} We were able to use a reliable low-cost alternative in LEDs, which have shown clinical success with PDT at various fluence rates.³⁴ An additional benefit of low-fluence light exposure is the reduction of photobleaching during treatment, and the LED did not show a significant effect on spheroid viability up to a 1 h exposure (Figure 2). While PS fluorescence after exposure to 20 J/cm^2 in LSFM (10 J/cm^2 , 2LT), it is still possible that some photobleaching occurred, regardless of the decreased fluence. The increase of irradiation time with a similar light source has also been shown to be suitable for *in vitro* PDT evaluation by Raza et al. (2020) in C8161 spheroids up to 3 h outside incubation conditions without adverse effects.³⁵

PDT treatments tend toward high fluence values in the clinic, such as those for ALA (30–540 J/cm^2 , >100 mW/cm^2) due to increased $^1\text{O}_2$ production.³⁶ However, this process is highly inefficient as oxygen is rapidly depleted during at least

40% of the total treatment duration.³⁷ High light intensity (mW/cm^2) causes rapid PS photobleaching, defined as the point at which $\sim 37\%$ of fluorescence signal strength is lost.³⁸ PpIX bleaching has been reported to vary, depending on the intensity of the light source, ranging from $5\text{--}150\text{ mW}/\text{cm}^2$ ($50\text{ J}/\text{cm}^2$) in a mouse skin model treated with ALA.³⁹ In comparison, lower power ($\sim 30\text{ mW}/\text{cm}^2$) has been shown to be equally effective at disrupting tumor growth while maintaining singlet oxygen production.⁴⁰ It is possible that oxygen depletion and subsequent hypoxia in the treated area may limit further PS activation as the concentration of immediately available O_2 is rapidly diminished after irradiation. Cells with low PS concentration or insufficient light exposure have been shown to have minimal PDT-induced death, even with high fluence ($360\text{ J}/\text{cm}^2$, $200\text{ mW}/\text{cm}^2$).⁴¹ The variations between these treatments could be due to steady PS bleaching due to a high-intensity light source, effectively reducing its effective concentration until oxygen consumption could keep up with available molecules in the tumor microenvironment. Seshadri et al. evaluated the effectiveness of PDT with high (100 mW) and low (7 mW) laser power regimens while adjusting PS concentrations. They did not observe a significant change in the total area of necrosis after PDT, observing intermittent hypoxia at 100 mW , ultimately leading to reduced effectiveness compared to 7 mW .⁴² This suggests that light delivery over extended periods of time with lower power improves PDT effectiveness.

The experimental conditions which were used in the present study paralleled those reported by Ouyang et al., where conditions were selected based on the ratio of early apoptotic to necrotic cells, corresponding to $4\text{ }\mu\text{g}/\text{mL}$ PpIX and $5\text{ J}/\text{cm}^2$.⁴³ Similarly, Zawacka-Pankau et al. showed $1\text{ }\mu\text{g}/\text{mL}$ PpIX ($2\text{ J}/\text{cm}^2$) caused a significant increase in p53-mediated and independent apoptosis in cancer cells through the activation of the HDM2-p53 complex.⁴⁴ In comparison to necrosis, apoptosis is generally thought to occur within a period of $12\text{--}24\text{ h}$ after signaling, though the exact duration is hard to determine as it depends on the activation pathway.⁴⁵ The structural and biological changes that spheroids undergo after PDT suggest that low-fluence PDT is capable of tumor destruction at nontoxic PS doses ($<5\text{ }\mu\text{g}/\text{mL}$). Debris is a dark halo surrounding the spheroid consisting of apoptotic and dead cells, which begins forming immediately after light exposure (Supporting Figure S3). Sustained damage to spheroids was also observed in all conditions, reflecting previous results, where spheroid viability was reduced for up to 72 h after PDT (Figure 3, Supporting Figures S2 and S3). While these conditions showed the best results (e.g., $10\text{ }\mu\text{g}/\text{mL}$ at $10\text{ J}/\text{cm}^2$, 1LT), it is worth noting that the influence of dark toxicity increases with higher PS concentrations ($>5\text{ }\mu\text{g}/\text{mL}$), which could misrepresent the efficiency of treatment conditions using $10\text{ }\mu\text{g}/\text{mL}$ PS as viability, and dsDNA content could be reduced up to $\sim 20\%$ before PDT.

Light fractionation in PDT has been proposed as a method for improving treatment outcomes without requiring the use of longer timescales for irradiation or higher drug doses, enabling reoxygenation while maintaining PS function and preventing photobleaching.⁴⁶ This method has shown positive results in preclinical trials, with 2-fold illumination treatments showing a markedly improved complete response rate compared to the control.¹⁵ Our results showed that 2LT conditions were significantly more effective than single treatments at most experimental conditions during the evaluation of LDH release

(Figure 3). In contrast, dsDNA quantification did not consistently show a significant difference between 1LT and 2LT, suggesting there are other factors which influence PDT efficiency because of light fractionation. Babilas et al. stated that fractionated PDT using PpIX ($25\text{--}100\text{ mW}/\text{cm}^2$) was less effective compared to single-dose treatments, possibly as a result of the 15 min interval between light doses.⁴⁷ Thus, we increased the time to a 24 h period, allowing reoxygenation and apoptosis to occur. Similar results were found by de Bruijn et al. using methyl-5-aminolevulinic acid (MAL) in a mouse skin model.¹⁶ Their work suggests PS localization before PDT is a key factor for both treatment effectiveness and determining the differences between single and multiple light doses.

Inefficient accumulation was shown to greatly diminish PDT effectiveness regardless of the total energy applied. de Bruijn et al. later observed PSs responded differently to light fractionation, suggesting sublethal damage to affected cells makes them more vulnerable to damage during the following treatments and highlighting the need for a more comprehensive evaluation of multiple PDT parameters.⁴⁸ The comparison between 1LT and 2LT shows a significant difference with LDH release, in contrast with dsDNA content, which is similar between treatments. This discrepancy may be influenced by the death of the proliferating outer cell layer during the first light treatment, which is followed by recruitment from viable quiescent cells located within the second spheroid layer. Proliferating cells are particularly susceptible to PDT due to their high uptake and oxygenation compared to inner sections.⁵¹ Samples also showed variation in uptake, with PpIX and PpIX-CD demonstrating penetration within the spheroid core after incubation, while PpIX@CD mostly accumulated in the outer layers. Millard et al. demonstrated the importance of carriers in their use of extracellular vesicles (EVs) for delivering liposomal meta-tetra(hydroxyphenyl)-chlorin (mTHPC). When loaded in EVs, mTHPC showed improved penetration in a cancer spheroid model after 24 h . In contrast, nonloaded mTHPC showed poor penetration regardless of incubation time, concentrating in the spheroid periphery.⁴⁹

The evaluation of drug uptake and localization within spheroids is key to obtaining insight into the behavior of PSs with various treatment combinations, as PDT efficiency is tied to not only the light dose but also drug concentration and localization. High uptake within the spheroids is desirable as it generally leads to enhanced phototoxicity, while inefficient accumulation results in low ROS production and higher cell survival. The main challenges associated with microscopy of spheroids are deformation or disruption before sectioning, light scattering, and low spatial resolution.⁵⁰ Light sheet fluorescence microscopy (LSFM) has been shown to be capable of analyzing spheroids up to 1 mm in diameter and determining drug penetration.⁵¹ Our data shows drug uptake was significantly impacted by concentration, coinciding with previous reports using porphyrins.²⁶ Spheroids exhibited significantly increased resistance to PDT, possibly due to slower cell proliferation and uneven PS distribution. This can be observed within most observed spheroid samples as fluorescence emissions rapidly decrease after $100\text{ }\mu\text{m}$ within the samples (Figure 5). Sample type also impacted the uptake, possibly due to aggregation during the incubation period. In contrast, cell monolayers typically exhibit uniform oxygen levels and PS uptake centered near the nuclei.¹⁰

The live/dead staining showed a high level of photoinduced damage on the outer spheroid layer and disruption of the spheroid structure with most conditions. The extent of damage was more apparent with the passage of time, with continuous loss of sphericity and diameter reduction observed in all spheroids up to 48 h after treatment. However, the decrease in spheroid size was not uniform among samples and showed variation, depending on the viewing angle. The visualization of damage using multiple viewing angles greatly improved the post-PDT assessment of treatment efficiency, showing large sections of spheroids having been sloughed off after PDT. Spheroids with single light exposures showed a significant reduction in thickness, with one side displaying high cell death and deformation as indicated by ethidium homodimer-1 staining, while the other showed more live cells, indicating that the PDT effect was mostly localized toward the side that faced the LED.

Spheroid damage after PDT can also be observed by the changes in surface roughness, which can indicate the amount of deposited extracellular matrix.⁵² The outer layers of spheroids appear to have been sloughed off and have not been reformed after 48 h post light exposure. This shedding has been observed in spheroids which have passed their stationary phase and is considered the start of their death phase.⁵³ Spheroids treated with 2LT showed a much more pronounced reduction in size and a higher degree of cell death than those with 1LT. This was expected as both LDH release and DNA content indicate lower sample viability with repeat light exposure. In summary, LSFM and SEM were able to show clear morphological changes after light activation. Spheroid thickness was consistently reduced with all samples and concentrations, though differential drug uptake may cause variation between samples with identical treatment conditions.

CONCLUSIONS

Currently, the gold standard for cancer drug testing is the *in vivo* tumor xenograft mouse model, which accurately replicates most tumor morphophysiological characteristics. However, animal models are not suitable for exploring the effect of individual treatment conditions due to their intrinsic complexity. Furthermore, large-scale screening experiments are costly, time-consuming, and face issues with ethical concerns. In this study, a total of 18 combinations of different PDT parameters (drug concentration, fluence, and light fractionation) were tested with two porphyrin functionalized carbon dot formulations (PpIX-CD, PpIX@CD) and compared to non-bound porphyrin (PpIX) totaling 54 combinations. These treatment conditions were evaluated using two different assays to determine the viability after PDT (LDH release and dsDNA quantification) and monitored at three time points (24, 48, and 72 h post-PDT). This led to the prescreening of unsuccessful PDT conditions such as 1 $\mu\text{g}/\text{mL}$ drug doses or 1LT, which would not have been apparent with only two-dimensional (2D) cell culture. Fractionated treatments (2LT) were shown to be significantly more effective compared to single treatments (1LT) regardless of other parameters. Furthermore, light sheet microscopy was used to obtain information regarding drug penetration into spheroids, with PpIX and PpIX-CD showing higher uptake compared to PpIX@CD. Spheroid morphology was also shown to be irregular due to varying response to PDT-induced damage, resulting in the shedding of the outer proliferating cell layer, which continued up to 48 h post-PDT. In conclusion, PDT parameter prescreening was able to rule

out multiple previously successful conditions with cell monolayers. The results presented herein highlight the importance of custom models tailored for PDT and the advantages of spheroids as a tool for screening treatment combinations to evaluate novel compounds.

ASSOCIATED CONTENT

Supporting Information

The Supporting Information is available free of charge at <https://pubs.acs.org/doi/10.1021/acsbiomaterials.1c00690>.

Sample properties summary table, PDT parameters table, LDH release, and total dsDNA content at 48/72 h post-PDT, comparison of light toxicity using relative PpIX concentration, uptake estimation through fluorescence, and LSFM images of spheroids treated with 5/10 $\mu\text{g}/\text{mL}$, 5/10 J/cm^2 , 1LT/2LT (PDF)

AUTHOR INFORMATION

Corresponding Author

Frederik Claeysens – University of Sheffield, Department of Materials Science and Engineering, Kroto Research Institute, Sheffield S3 7HQ, United Kingdom; INSIGNEO Institute for In Silico Medicine, University of Sheffield, Sheffield S1 3JD, United Kingdom; orcid.org/0000-0002-1030-939X; Email: f.claeysens@sheffield.ac.uk

Authors

Jose R. Aguilar Cosme – University of Sheffield, Department of Materials Science and Engineering, Kroto Research Institute, Sheffield S3 7HQ, United Kingdom; INSIGNEO Institute for In Silico Medicine, University of Sheffield, Sheffield S1 3JD, United Kingdom; orcid.org/0000-0001-7933-3905

Dan C. Gagui – Department of Oncology and Metabolism, The Medical School, University of Sheffield, Sheffield S10 2RX, United Kingdom; INSIGNEO Institute for In Silico Medicine, University of Sheffield, Sheffield S1 3JD, United Kingdom

Nicola H. Green – University of Sheffield, Department of Materials Science and Engineering, Kroto Research Institute, Sheffield S3 7HQ, United Kingdom; INSIGNEO Institute for In Silico Medicine, University of Sheffield, Sheffield S1 3JD, United Kingdom

Helen E. Bryant – Department of Oncology and Metabolism, The Medical School, University of Sheffield, Sheffield S10 2RX, United Kingdom

Complete contact information is available at:

<https://pubs.acs.org/doi/10.1021/acsbiomaterials.1c00690>

Author Contributions

The manuscript was written through contributions of all authors. All authors have given approval to the final version of the manuscript. J.R.A.C.: Conceptualization, Data curation (equal), Formal analysis, Funding acquisition (supporting), Investigation (lead), Methodology (lead), Project administration (lead), Resources (equal), Supervision (supporting), Validation (lead), Visualization (lead), Writing—original draft (lead), Writing—review & editing (equal). D.C.G.: Data curation (equal), Investigation (supporting), Visualization (supporting), Writing—Original draft (supporting). N.H.G.: Methodology (equal), Resources (supporting), Validation (supporting), Writing—review & editing (equal). H.E.B.:

Methodology (equal), Supervision (equal), Validation (supporting), Writing—review & editing (equal). F.C.: Funding acquisition (lead), Resources (equal) Methodology (equal), Supervision (equal), Validation (supporting), Writing—review & editing (equal).

Notes

The authors declare no competing financial interest.

ACKNOWLEDGMENTS

This work was supported by a grant from the Mexican Federal Government through the National Council of Science and Technology (426851) and Innovation and Technological Transfer of Nuevo Leon (CVU-610782). J.R.A.C. and D.C.G. acknowledge financial support from the INSIGNEO Institute for in Silico Medicine. We also acknowledge the Henry Royce Institute for Advanced Materials, funded through EPSRC grants EP/R00661X/1, EP/S019367/1, EP/P02470X/1, and EP/P025285/1, for access to the ZEISS Lightsheet Z.1 at the University of Sheffield. The authors are thankful for the Electron Microscopy Unit, the University of Sheffield, for the use of SEM.

ABBREVIATIONS

1LT, single light treatment; $^1\text{O}_2$, singlet oxygen; 2LT, double light treatment; 3D, three-dimensional; ALA, aminolevulinic acid; CD, carbon dot; dsDNA, double stranded DNA; LDH, lactate dehydrogenase; LM, light microscopy; LSFM, light sheet fluorescence microscopy; MAL, methyl-5-aminolevulinate; MCTS, multicellular cancer spheroids; MWCO, molecular weight cutoff; PpIX, protoporphyrin IX; PS, photosensitizer; PDT, photodynamic therapy

REFERENCES

- (1) Kim, M. M.; Darafsheh, A. Light Sources and Dosimetry Techniques for Photodynamic Therapy. *Photochem. Photobiol.* **2020**, *96*, 280–294.
- (2) Dąbrowski, J. M.; Arnaut, L. G. Photodynamic Therapy (PDT) of Cancer: From Local to Systemic Treatment. *Photochem. Photobiol. Sci.* **2015**, *1765*–1780.
- (3) Kiesslich, T.; Gollmer, A.; Maisch, T.; Berneburg, M.; Plaetzer, K. A Comprehensive Tutorial on in Vitro Characterization of New Photosensitizers for Photodynamic Antitumor Therapy and Photodynamic Inactivation of Microorganisms. *Biomed. Res. Int.* **2013**, *1*–17.
- (4) Allison, R. R.; Mota, H. C.; Sibata, C. H. Clinical PD/PDT in North America: An Historical Review. *Photodiagn. Photodyn. Ther.* **2004**, *1*, 263–277.
- (5) Zhang, J.; Jiang, C.; Figueiró Longo, J. P.; Azevedo, R. B.; Zhang, H.; Muehlmann, L. A. An Updated Overview on the Development of New Photosensitizers for Anticancer Photodynamic Therapy. *Acta Pharm. Sin. B* **2018**, *137*–146.
- (6) Crous, A.; Abrahamse, H. Effective Gold Nanoparticle-Antibody-Mediated Drug Delivery for Photodynamic Therapy of Lung Cancer Stem Cells. *Int. J. Mol. Sci.* **2020**, *21*, No. 3742.
- (7) Laroui, N.; Coste, M.; Lichon, L.; Bessin, Y.; Gary-Bobo, M.; Pratiel, G.; Bonduelle, C.; Bettache, N.; Ulrich, S. Combination of Photodynamic Therapy and Gene Silencing Achieved through the Hierarchical Self-Assembly of Porphyrin-SiRNA Complexes. *Int. J. Pharm.* **2019**, *569*, No. 118585.
- (8) Song, Y.; Wang, L.; Xie, Z. Metal–Organic Frameworks for Photodynamic Therapy: Emerging Synergistic Cancer Therapy. *Biotechnol. J.* **2021**, *16*, No. 1900382.
- (9) Lee, S. Y.; Lee, R.; Kim, E.; Lee, S.; Park, Y. II. Near-Infrared Light-Triggered Photodynamic Therapy and Apoptosis Using

Upconversion Nanoparticles With Dual Photosensitizers. *Front. Bioeng. Biotechnol.* **2020**, *0*, No. 275.

(10) Aguilar Cosme, J. R.; Bryant, H. E.; Claeysens, F. Carbon Dot-Protoporphyrin IX Conjugates for Improved Drug Delivery and Bioimaging. *PLoS One* **2019**, *14*, No. e0220210.

(11) McKenzie, L. K.; Sazanovich, I. V.; Baggaley, E.; Bonneau, M.; Guerchais, V.; Williams, J. A. G.; Weinstein, J. A.; Bryant, H. E. Metal Complexes for Two-Photon Photodynamic Therapy: A Cyclometallated Iridium Complex Induces Two-Photon Photosensitization of Cancer Cells under Near-IR Light. *Chem. - Eur. J.* **2017**, *23*, 234–238.

(12) Li, Y.; Zheng, X.; Zhang, X.; Liu, S.; Pei, Q.; Zheng, M.; Xie, Z. Porphyrin-Based Carbon Dots for Photodynamic Therapy of Hepatoma. *Adv. Healthcare Mater.* **2017**, *6*, No. 1600924.

(13) Silva, Z. S.; Bussadori, S. K.; Santos Fernandes, K. P.; Huang, Y. Y.; Hamblin, M. R. Animal Models for Photodynamic Therapy (PDT). *Biosci. Rep.* **2015**, No. e00265.

(14) Tetaud, M. C.; Vermandel, M.; Leroy, H. A.; Leroux, B.; Maurage, C. A.; Lejeune, J. P.; Mordon, S.; Reyns, N. Interstitial 5-ALA Photodynamic Therapy and Glioblastoma: Preclinical Model Development and Preliminary Results. *Photodiagn. Photodyn. Ther.* **2016**, *13*, 218–224.

(15) de Vijlder, H. C.; Sterenborg, H. J. C. M.; Martino Neumann, H. A.; Robinson, D. J.; de Haas, E. R. M. Light Fractionation Significantly Improves the Response of Superficial Basal Cell Carcinoma to Aminolaevulinic Acid Photodynamic Therapy: Five-Year Follow-up of a Randomized, Prospective Trial. *Acta Derm.-Venereol.* **2012**, *92*, 641–647.

(16) de Bruijn, H. S.; de Haas, E. R. M.; Hebeda, K. M.; van der Ploeg - Van Den Heuvel, A.; Sterenborg, H. J. C. M.; Neumann, H. A. M.; Robinson, D. J. Light Fractionation Does Not Enhance the Efficacy of Methyl 5-Aminolevulinate Mediated Photodynamic Therapy in Normal Mouse Skin. *Photochem. Photobiol. Sci.* **2007**, *6*, 1325–1331.

(17) Weiswald, L. B.; Bellet, D.; Dangles-Marie, V. Spherical Cancer Models in Tumor Biology. *Neoplasia* **2015**, *1*–15.

(18) Vaira, V.; Fedele, G.; Pyne, S.; Fasoli, E.; Zadra, G.; Bailey, D.; Snyder, E.; Favarsani, A.; Coggi, G.; Flavin, R.; Bosari, S.; Loda, M. Preclinical Model of Organotypic Culture for Pharmacodynamic Profiling of Human Tumors. *Proc. Natl. Acad. Sci. U.S.A.* **2010**, *107*, 8352–8356.

(19) Severyukhina, A. N.; Petrova, N. V.; Smuda, K.; Terentyuk, G. S.; Klebtsov, B. N.; Georgieva, R.; Bäumlner, H.; Gorin, D. A. Photosensitizer-Loaded Electrospun Chitosan-Based Scaffolds for Photodynamic Therapy and Tissue Engineering. *Colloids Surf., B* **2016**, *144*, 57–64.

(20) Phan, N.; Hong, J. J.; Tofig, B.; Mapua, M.; Elashoff, D.; Moatamed, N. A.; Huang, J.; Memarzadeh, S.; Damoiseaux, R.; Soragni, A. A Simple High-Throughput Approach Identifies Actionable Drug Sensitivities in Patient-Derived Tumor Organoids. *Commun. Biol.* **2019**, *2*, No. 78.

(21) Gong, X.; Lin, C.; Cheng, J.; Su, J.; Zhao, H.; Liu, T.; Wen, X.; Zhao, P. Generation of Multicellular Tumor Spheroids with Microwell-Based Agarose Scaffolds for Drug Testing. *PLoS One* **2015**, *10*, No. e0130348.

(22) Hagemann, J.; Jacobi, C.; Hahn, M.; Schmid, V.; Welz, C.; Schwenk-Zieger, S.; Stauber, R.; Baumeister, P.; Becker, S. Spheroid-Based 3D Cell Cultures Enable Personalized Therapy Testing and Drug Discovery in Head and Neck Cancer. *Anticancer Res.* **2017**, *37*, 2201–2210.

(23) Ham, S. L.; Joshi, R.; Thakuri, P. S.; Tavana, H. Liquid-Based Three-Dimensional Tumor Models for Cancer Research and Drug Discovery. *Exp. Biol. Med.* **2016**, *241*, 939–954.

(24) Mehta, G.; Hsiao, A. Y.; Ingram, M.; Luker, G. D.; Takayama, S. Opportunities and Challenges for Use of Tumor Spheroids as Models to Test Drug Delivery and Efficacy. *J. Controlled Release* **2012**, *164*, 192–204.

- (25) Kim, S.-H.; Kuh, H.-J.; Dass, C. R. The Reciprocal Interaction: Chemotherapy and Tumor Microenvironment. *Curr. Drug Discovery Technol.* **2011**, *8*, 102–106.
- (26) Pereira, P. M. R.; Berisha, N.; Bhupathiraju, N. V. S. D. K.; Fernandes, R.; Tomé, J. P. C.; Drain, C. M. Cancer Cell Spheroids Are a Better Screen for the Photodynamic Efficiency of Glycosylated Photosensitizers. *PLoS One* **2017**, *12*, No. e0177737.
- (27) Gunay, G.; Kirit, H. A.; Kamatar, A.; Baghdasaryan, O.; Hamsici, S.; Acar, H. The Effects of Size and Shape of the Ovarian Cancer Spheroids on the Drug Resistance and Migration. *Gynecol. Oncol.* **2020**, *159*, 563–572.
- (28) Tchoryk, A.; Taresco, V.; Argent, R. H.; Ashford, M.; Gellert, P. R.; Stolnik, S.; Grabowska, A.; Garnett, M. C.; Gellert, P. R. Penetration and Uptake of Nanoparticles in 3D Tumor Spheroids. *Bioconjugate Chem.* **2019**, *30*, 1371–1384.
- (29) Sriraman, S. K.; Aryasomayajula, B.; Torchilin, V. P. Barriers to Drug Delivery in Solid Tumors. *Tissue Barriers* **2014**, No. e29528.
- (30) Däster, S.; Amatruda, N.; Calabrese, D.; Ivanek, R.; Turrini, E.; Droeser, R. A.; Zajac, P.; Fimognari, C.; Spagnoli, G. C.; Iezzi, G.; Mele, V.; Muraro, M. G. Induction of Hypoxia and Necrosis in Multicellular Tumor Spheroids Is Associated with Resistance to Chemotherapy Treatment. *Oncotarget* **2017**, *8*, 1725–1736.
- (31) Friedrich, J.; Seidel, C.; Ebner, R.; Kunz-Schughart, L. A. Spheroid-Based Drug Screen: Considerations and Practical Approach. *Nat. Protoc.* **2009**, *4*, 309–324.
- (32) Helander, L.; Krokan, H. E.; Johnsson, A.; Gederaas, O. A.; Plaetzer, K. Red versus Blue Light Illumination in Hexyl 5-Aminolevulinic Acid Photodynamic Therapy: The Influence of Light Color and Irradiance on the Treatment Outcome in Vitro. *J. Biomed. Opt.* **2014**, *19*, No. 088002.
- (33) Mathews, M. S.; Angell-Petersen, E.; Sanchez, R.; Sun, C. H.; Vo, V.; Hirschberg, H.; Madsen, S. J. The Effects of Ultra Low Fluence Rate Single and Repetitive Photodynamic Therapy on Glioma Spheroids. *Lasers Surg. Med.* **2009**, *41*, 578–584.
- (34) Hempstead, J.; Jones, D. P.; Ziouche, A.; Cramer, G. M.; Rizvi, I.; Arnason, S.; Hasan, T.; Celli, J. P. Low-Cost Photodynamic Therapy Devices for Global Health Settings: Characterization of Battery-Powered LED Performance and Smartphone Imaging in 3D Tumor Models. *Sci. Rep.* **2015**, *5*, No. 10093.
- (35) Raza, A.; Archer, S. A.; Fairbanks, S. D.; Smitten, K. L.; Botchway, S. W.; Thomas, J. A.; Macneil, S.; Haycock, J. W. A Dinuclear Ruthenium(II) Complex Excited by Near-Infrared Light through Two-Photon Absorption Induces Phototoxicity Deep within Hypoxic Regions of Melanoma Cancer Spheroids. *J. Am. Chem. Soc.* **2020**, *142*, 4639–4647.
- (36) Peng, Q.; Warloe, T.; Berg, K.; Moan, J.; Kongshaug, M.; Giercksky, K.; Nesland, J. M. 5-Aminolevulinic Acid-based Photodynamic Therapy. *Cancer* **1997**, *79*, 2282–2308.
- (37) Henderson, B. W.; Busch, T. M.; Vaughan, L. A.; Frawley, N. P.; Babich, D.; Sosa, T. A.; Zollo, J. D.; Dee, A. S.; Cooper, M. T.; Bellnier, D. A.; Greco, W. R.; Oseroff, A. R. Photofrin Photodynamic Therapy Can Significantly Deplete or Preserve Oxygenation in Human Basal Cell Carcinomas during Treatment, Depending on Fluence Rate. *Cancer Res.* **2000**, *60*, 525–529.
- (38) Jarvi, M. T.; Patterson, M. S.; Wilson, B. C. Insights into Photodynamic Therapy Dosimetry: Simultaneous Singlet Oxygen Luminescence and Photosensitizer Photobleaching Measurements. *Biophys. J.* **2012**, *102*, 661–671.
- (39) Robinson, D. J.; De Bruijn, H. S.; Van Der Veen, N.; Stringer, M. R.; Brown, S. B.; Star, W. M. Fluorescence Photobleaching of ALA-Induced Protoporphyrin IX during Photodynamic Therapy of Normal Hairless Mouse Skin: The Effect of Light Dose and Irradiance and the Resulting Biological Effect. *Photochem. Photobiol.* **1998**, *67*, 140–149.
- (40) Korbelik, M.; Kros, G.; Kros, J.; Dougherty, G. J. The Role of Host Lymphoid Populations in the Response of Mouse EMT6 Tumor to Photodynamic Therapy. *Cancer Res.* **1996**, *56*, 5647–5652.
- (41) Foster, T. H.; Murant, R. S.; Bryant, R. G.; Knox, R. S.; Gibson, S. L.; Hilf, R. Oxygen Consumption and Diffusion Effects in Photodynamic Therapy. *Radiat. Res.* **1991**, *126*, 296.
- (42) Seshadri, M.; Bellnier, D. A.; Vaughan, L. A.; Sperry, J. A.; Mazurchuk, R.; Foster, T. H.; Henderson, B. W. Light Delivery over Extended Time Periods Enhances the Effectiveness of Photodynamic Therapy. *Clin. Cancer Res.* **2008**, *14*, 2796–2805.
- (43) Ouyang, G.; Xiong, L.; Liu, Z.; Lam, B.; Bui, B.; Ma, L.; Chen, X.; Zhou, P.; Wang, K.; Zhang, Z.; Huang, H.; Miao, X.; Chen, W.; Wen, Y. Inhibition of Autophagy Potentiates the Apoptosis-Inducing Effects of Photodynamic Therapy on Human Colon Cancer Cells. *Photodiagn. Photodyn. Ther.* **2018**, *21*, 396–403.
- (44) Zawacka-Pankau, J.; Issaeva, N.; Hossain, S.; Pramanik, A.; Selivanova, G.; Podhajski, A. J. Protoporphyrin IX Interacts with Wild-Type P53 Protein in Vitro and Induces Cell Death of Human Colon Cancer Cells in a P53-Dependent and -Independent Manner. *J. Biol. Chem.* **2007**, *282*, 2466–2472.
- (45) Green, D. R. Apoptotic Pathways: Ten Minutes to Dead. *Cell* **2005**, *671*–674.
- (46) Pogue, B. W.; Braun, R. D.; Lanzen, J. L.; Erickson, C.; Dewhirst, M. W. Analysis of the Heterogeneity of PO₂ Dynamics During Photodynamic Therapy with Verteporfin. *Photochem. Photobiol.* **2001**, *74*, 700.
- (47) Babilas, P.; Schacht, V.; Liebsch, G.; Wolfbeis, O. S.; Landthaler, M.; Szeimies, R. M.; Abels, C. Effects of Light Fractionation and Different Fluence Rates on Photodynamic Therapy with 5-Aminolaevulinic Acid in Vivo. *Br. J. Cancer* **2003**, *88*, 1462–1469.
- (48) de Bruijn, H. S.; Brooks, S.; Van Der Ploeg-Van Den Heuvel, A.; Ten Hagen, T. L. M.; De Haas, E. R. M.; Robinson, D. J. Light Fractionation Significantly Increases the Efficacy of Photodynamic Therapy Using BF-200 ALA in Normal Mouse Skin. *PLoS One* **2016**, *11*, No. e0148850.
- (49) Millard, M.; Posty, S.; Piffoux, M.; Jasniewski, J.; Lassalle, H.-P.; Yakavets, I.; Gazeau, F.; Wilhelm, C.; Silva, A. K. A.; Bezdetnaya, L. MTHPC-Loaded Extracellular Vesicles Significantly Improve MTHPC Diffusion and Photodynamic Activity in Preclinical Models. *Pharmaceutics* **2020**, *12*, No. 676.
- (50) Pampaloni, F.; Ansari, N.; Stelzer, E. H. K. High-Resolution Deep Imaging of Live Cellular Spheroids with Light-Sheet-Based Fluorescence Microscopy. *Cell Tissue Res.* **2013**, 161–177.
- (51) Lazzari, G.; Vinciguerra, D.; Balasso, A.; Nicolas, V.; Goudin, N.; Garfa-Traore, M.; Fehér, A.; Dinnyés, A.; Nicolas, J.; Couvreur, P.; Mura, S. Light Sheet Fluorescence Microscopy versus Confocal Microscopy: In Quest of a Suitable Tool to Assess Drug and Nanomedicine Penetration into Multicellular Tumor Spheroids. *Eur. J. Pharm. Biopharm.* **2019**, *142*, 195–203.
- (52) Amaral, R. L. F.; Miranda, M.; Marcato, P. D.; Swiech, K. Comparative Analysis of 3D Bladder Tumor Spheroids Obtained by Forced Floating and Hanging Drop Methods for Drug Screening. *Front. Physiol.* **2017**, *8*, No. 605.
- (53) Leek, R. D.; Stratford, I.; Harris, A. L. The Role of Hypoxia-Inducible Factor-1 in Three-Dimensional Tumor Growth, Apoptosis, and Regulation by the Insulin-Signaling Pathway. *Cancer Res.* **2005**, *65*, 4147–4152.